Desalination and Water Treatment
www.deswater.com

doi:10.5004/dwt.2019.24116

159 (2019) 250–256
August

Synthesis, characterization, and photo-catalytic activity of Ag/ZnO/SBA-15 composite

Yao Zhou

College of Environment and Safety Engineering, Qingdao University of Science and Technology, Qingdao 266042, China, email: 116708013@qq.com (Y. Zhou)

Received 12 October 2018; Accepted 9 March 2019

ABSTRACT

Herein, the mesoporous silica material SBA-15 was chosen as a carrier to load photo-catalytic composite materials. To promote the catalytic activity of ZnO under solar light, photo-reduced Ag/ZnO materials were synthesized onto SBA-15. These composite materials were unambiguously characterized using a variety of spectroscopic techniques. The adsorption and catalytic efficiencies of these catalysts were evaluated by the decomposition of Methyl Orange (MO). The resulting material showed enhanced photo-catalytic efficiency with 96% MO degradation using just simulated solar-light irradiation over 60 min. With excellent stability and recyclability, Ag/ZnO/SBA-15 represents a promising photo-catalyst for decontamination applications.

Keywords: SBA-15; Ag/ZnO; Photocatalysis; MO

1. Introduction

Zinc oxide (ZnO) is a common photo-catalytic material because it possesses a band gap similar to that of titanium dioxide (TiO_2). With excellent properties such as low cost and high photo-catalytic efficiency, ZnO has attracted significant research efforts in the field of pollutant degradation[1–4]. However, due to its wide band gap (3.2 eV) and low surface area, utilization of ZnO materials have been limited [5–7]. Many studies have illustrated the drawbacks of using ZnO.

Among those studies, the unique optical and electronic properties of noble metal incorporation are favorably viewed as an effective way to promote the enhancement of photo-catalytic activity and has attracted considerable research interest [8].

Of the many carriers with beneficial surface properties, mesoporous silicate SBA-15 is generally selected as a support for photo-catalytic materials due to its thermal stability and large surface area among other beneficial properties [9,10].

Recently, environmental protection is one of the great challenges in the world. Organic dyes not readily degraded have led to a number of potential environmental problems. Methyl orange (MO) is a common dye widely used in industry manufacture due to its stability [11]. Many publications have reported the decomposition of MO using various photo-catalysts using either ultraviolet or solar irradiation [12].

In this work, Ag/ZnO/SBA-15 was photo-reduced and hydrothermally synthesized. The catalytic performance of this Ag/ZnO/SBA-15 nano-material was evaluated for MO degradation under visible light irradiation in 60 min. A systematic analysis utilizing several modern techniques was undertaken to study the relationship between its micro-structure and catalytic efficiency under visible light.

2. Experimental

2.1. Materials

ZnO, $AgNO_3$, Zn $(NO_3)_2$, H_2O_2, NaOH and HNO_3 were obtained from China Tianjin Fuchen Chemical Reagent Factory. Tetraethyl orthosilicate (TEOS) and 3-aminopropyltrimethoxysilane (APTMS) were provided by Nanjing Chemical Company. All purchased regents were analytical grade purity.

*Corresponding author.

2.2. Photo-catalyst fabrication

The mesoporous silica SBA-15 was synthesized first [13]. NH_2-SBA-15 was synthesized by functionalizing the amine to connect the ZnO photo-catalyst onto the SBA-15 surface [14]. Afterwards, 0.1 g of the NH_2-SBA-15 support was added to 100 mL of a 0.1 M solution of $Zn(NO_3)_2$ and heated in a water bath at 80°C for 4 h. The amino-functionalization of SBA-15 bound the ZnO catalyst in solution. The pH was adjusted to 13.0 by adding NaOH and HNO_3 [2], creating an alkaline environment for zinc oxide hydrolysis. After filtration and drying, the ZnO/SBA-15 mixture and 50 mL of 0.05 M $AgNO_3$ were combined. After irradiation by visible light ($\lambda > 400$ nm) for 4 h, the adsorbed Ag^+ was photocatalytically reduced to metallic Ag [15] which was then rinsed and dried. For purposes of comparison to Ag/ZnO/SBA-15, pure Ag/ZnO was synthesized using a same procedure except for the addition of SBA-15 and the ZnO was purchased.

2.3. Characterization

X-ray diffraction patterns for the photo-catalyst were measured on a diffractometer (D/MAX-RB, Japan) 2θ values ranged from 0 to 60° with a scanning rate of 2°/min, at a voltage of 40 kV and current of 50 mA. Transmission electron microscopy (TEM) images were recorded on a JEOL JEM-2100F. Elemental composition of the Ag/ZnO/SBA-15 photo-catalyst was conducted with energy dispersive spectroscopy (EDS) equipped on TEM. The valences of the various elements in Ag/ZnO/SBA-15 were detected using XPS analysis (Thermo VG Multilab 2000). The pore and surface structures of the sample were measured at by a N_2 isothermal-adsorption instrument (ASAP2010). Diffuse reflectance spectra of the samples were obtained on an UV-Vis spectrophotometer (Sinco S-4100).

2.4. Evaluation of adsorption and catalytic activities

Prior to each photo-catalytic test, evaluation of the adsorption effect conducted by stirring the catalyst/solution mixture for 60 min in the dark. After adsorption, 100 mL of 20 mg/L Methyl Orange (MO) was used as a typical organic contaminant for detecting the photo-catalytic activities of the three samples under simulated solar irradiation. The photo-degradation of MO took place in a glass reactor equipped with an XG500 xenon long-arc lamp which was temperature controlled at 30°C using a water circulation bath. The light intensity was approximately 25 mW/cm^2 and the distance from the xenon lamp to the reactor was 15 cm. Approximately 50 mg of sample was added to each reactor. The photo-catalytic tests were then carried out under visible light both with and without H_2O_2 and argon gas. Aliquots of the solution (~ 5 mL) were extracted at each interval and then analyzed by UV-Vis for absorbance 464 nm.

The degradation of MO was estimated using the expression $C_0 - C/C_0$, where C_0 was the initial concentration and C was the degradation concentration measured at each interval. As the concentration of MO was linearly proportional to the absorbance value (A) at 464 nm, the equation $A_0 - A/A_0 = C_0 - C/C_0$ was obtained.

3. Results and discussion

3.1. Structure analysis

The low angle XRD patterns of pure SBA-15 and NH_2-SBA-15 are illustrated in Fig. 1A. Three peaks resulting from the (100), (110) and (200) reflections belonged to a two-dimensional hexagonal lattice structure [2]. The peak at (100) was also obtained for the amino-functioned sample, but with an obvious decrease due to functionalization and indicated a decrease in the high order of the mesoporous material.

The phase characteristics of Ag/ZnO/SBA-15 were studied using X-ray diffraction (XRD). The broad peak at approximately 25° shown in Fig. 1B may be attributed to amorphous SiO_2 in SBA-15 [15]. The 2θ peaks at 31.78°, 56.62° and 47.56° of ZnO (wurtzite phase, JCPDS No. 361451) as well as the 2θ peak at 38.14° and 64.42° for metallic Ag (JCPDS No. 040783) indicated that the Ag/ZnO composite had been prepared. These results suggested that metallic Ag was produced during the photo-reduction process.

3.2. Morphology and elemental analysis of the photo-catalyst

The morphology of Ag/ZnO/SBA-15 is shown in Fig. 2A, showing the typical pore array structure of the

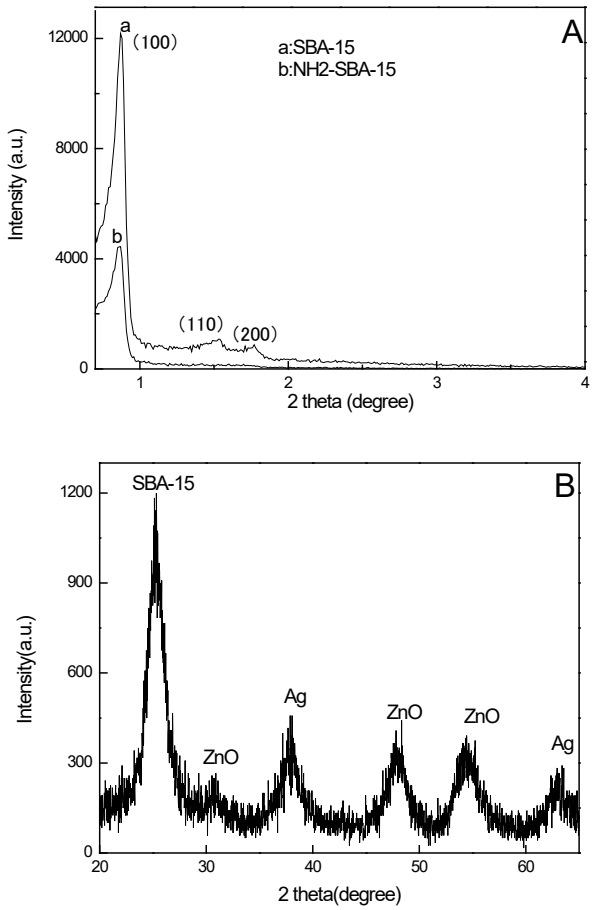

Fig. 1. XRD patterns. A: SBA-15 and NH_2-SBA-15; B: Ag/ZnO/SBA-15.

sample. The catalysts are on the SBA-15 surface. The HRTEM image of a Ag/ZnO composite loaded on the surface of SBA-15 can be seen in Fig. 2B. From the image, lattice spacings of d_{101} = 0.246 nm and d_{111} = 0.238 nm are consistent with the interplanar spacings of ZnO and Ag, respectively (JCPDS No. 361451, JCPDS No. 040783). The particle sizes of Ag and ZnO are approximately 5 nm and 10 nm, respectively.

Energy dispersive X-ray spectroscopy (EDX) is a well-known technique used for surface sample elemental analyses. Analysis of EDX results shown in Fig. 2C and Table 1 reveals the co-existence of Zn, Ag, O and Si; this confirms the formation of the Ag/ZnO/SBA-15 composite.

3.3. N_2 adsorption-desorption, XPS analysis and optical properties of the photo-catalysts

The N_2 adsorption-desorption isotherms of the three samples at 77K exhibited step wise adsorption behavior as shown in Fig. 3A. Type IV adsorption-desorption isotherm characteristics were observed for all three samples and indicated the uniformity of mesoporous materials [16]. The pore size distribution shown in Fig. 3A (insert curves) also confirmed that these materials are mesoporous.

In addition, when the relative pressure P/P_0 was 0.6, the adsorbed N_2 volume decreased in all three samples: pure SBA-15, ZnO/SBA-15 and Ag/ZnO/SBA-15. The insert curve shown in Fig. 3A illustrates the pore-size distribution, measured by the BJH method [17]. Due to ZnO or Ag dispersion on the SBA-15 surface, there was a reduction in the textural and structural properties from the analysis results shown in Table. 1. One explanation for these results could be that some of the crystals blocked the mesoporous material channels during synthesis. In general, the two photo-catalytic materials loaded on SBA-15 still retained their mesoporous structure. The mesoporous characteristics of the modified materials improved photo-catalytic performance.

XPS analysis was used to study the valence of Ag on Ag/ZnO/SBA-15. Fig. 3B shows two peaks – 368.5 eV and 374.4 eV, assigned to the Ag 3d5/2 and Ag 3d3/2 binding energies, respectively. A spin energy separation of ~ 6.1 eV between the two peaks further indicated that there was zero-valent Ag in the composite [18].

The optical properties of the two samples are illustrated in Fig. 3C which shows that ZnO/SBA-15 has a strong absorption at approximately 340 nm. Because of the surface plasmon resonance (SPR) of Ag nano-particles [19], the Ag/ZnO/SBA-15 composite exhibited an intensive absorption band from 400–700 nm.

3.4. Absorption behavior

MO adsorbs onto Ag/ZnO/SBA-15, ZnO/SBA-15, Ag/ZnO, NH_2-SBA-15 and pure SBA-15 in the dark. The initial concentration of MO was 20 mg/L; the samples were 2 g/L. As seen in Fig. 4, the adsorption activities of all five samples were low and the adsorption activity of pure SBA-15 was also limited. Thus, pure SBA-15 did significantly factor into this process. Fig. 4 also shows that the adsorption activities of Ag/ZnO/SBA-15 and ZnO/SBA-15 were not much higher, either.

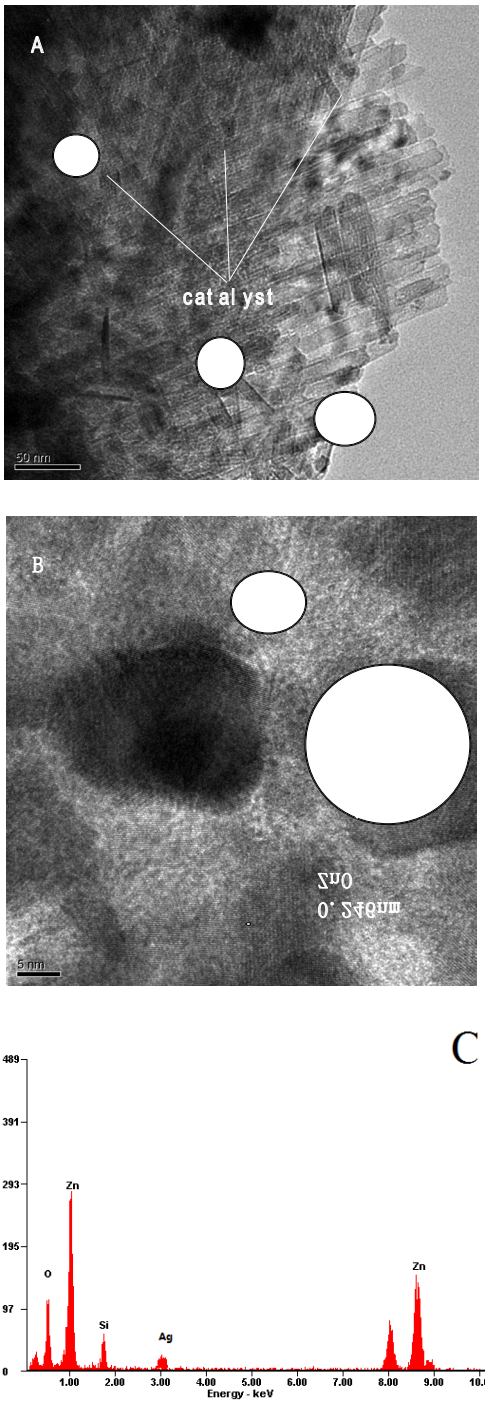

Fig. 2. TEM images. A: The morphology; B: HRTEM images of Ag/ZnO/SBA-15; C: EDX spectrum of Ag/ZnO/SBA-15 composite.

3.5. Catalytic performance

MO was used as a model pollutant to test the catalytic performances of all three samples. Fig. 5 shows the degradation of MO under different conditions for all three samples. These results showed that there was no MO degradation using only visible light irradiation for 60 min.

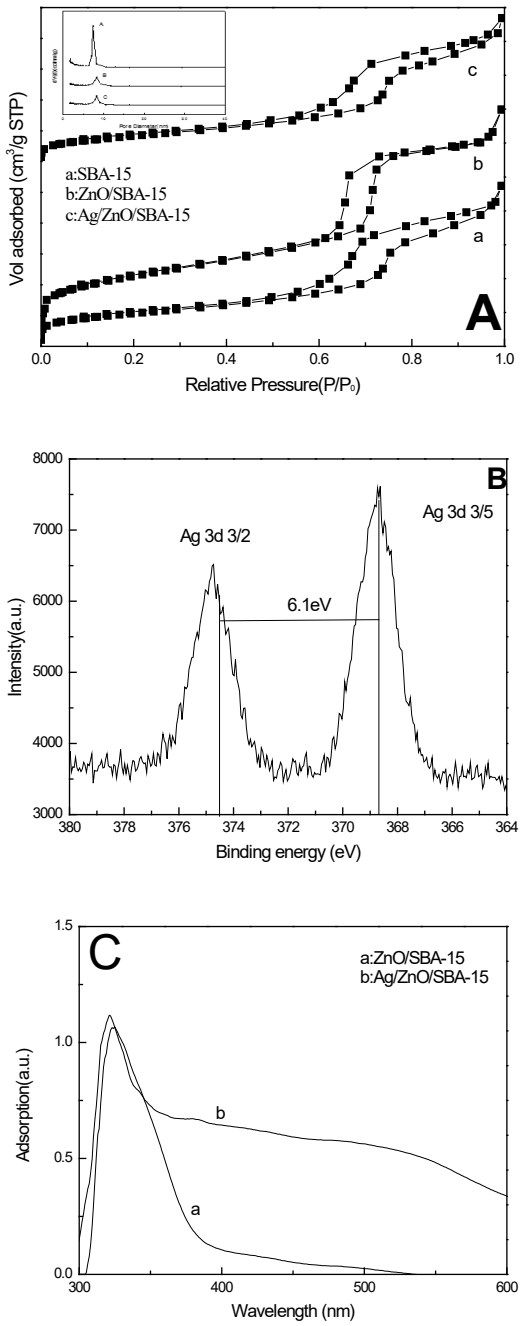

Fig. 3. N_2 adsorption-desorption, Ag 3d XPS spectra and UV-Vis absorption properties.

Table 1
EDX results of Ag/ZnO/SBA-15

Element	Atomic %
O	29.19
Zn	25.85
Ag	13.12
Si	30.84
Total	100.0

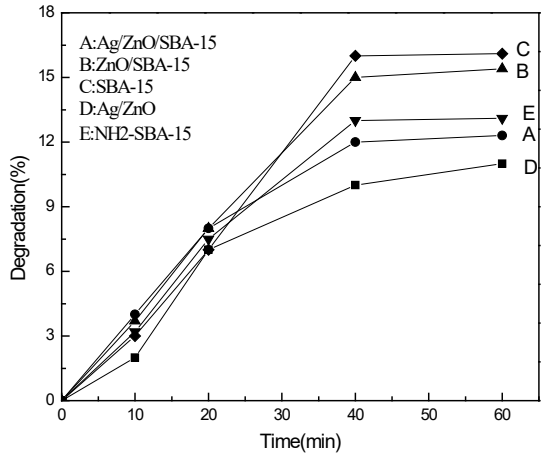

Fig. 4. Absorption behavior of MO in darkness.

The degradation activity of MO by Ag/ZnO/SBA-15 using visible light was greater than that for ZnO/SBA-15 and Ag/ZnO, indicating that Ag loading was an effective way to improve photo-catalytic performance. The mesoporous structure of SBA-15 benefited the photo-catalytic degradation of MO as well; however, MO degradation increased significantly when H_2O_2 was added to MO. For instance, Ag/ZnO/SBA-15 degraded approximately ~96% of MO using visible light in the presence of H_2O_2 over the course of 60 min. In contrast, when the same reaction with Ag/ZnO/SBA-15 was run with simulated solar radiation under argon gas, only 42% of MO degraded.

In order to examine the potential reaction mechanism and determine the primary reactive species during photo-catalysis, radical scavengers were added to the reaction mixture (Fig. 6). For those experiments, terephthalic acid was used to scavenge the ·OH radical [20], EDTA for the H^+ ion [21] and p-benzoquinone quenched $\cdot O_2$ [22]. Fig. 6 shows the photo-catalytic activities of the Ag/ZnO/SBA-15 composite using these different scavengers. As shown to all, methanol did not lead significant decreases in photo-catalytic activities; however, EDTA and p-benzoquinone nearly completely inhibited the removal of MO. These results suggested that H^+ and $\cdot O_2$ were the primary reactive species during photo-catalysis.

ZnO/SBA-15 has weak photo-catalytic activity under visible light due to its limited absorption in the visible region (Fig. 3C). Mo degradation under simulated solar radiation was virtually nonexistent for the ZnO/SBA-15 system; this is likely due to its band gap energy of 3.2 eV [3]. The Ag/ZnO/SBA-15 hetero-structure sample showed much higher photo-catalytic activities because of the surface plasmon resonance of metallic Ag particles.

When radiated by UV or visible light equal to or surpassing the semiconductor band gap, the electron-hole pairs of the photo-catalyst were synthesized and separated on the semiconductor [23]. When the Ag/ZnO hetero-structure nano-catalyst was dispersed in the solution with MO, the Schottky barrier at the Ag/ZnO interface formed in the presence of visible light [24]. The Ag particles on the ZnO surface were described as a sink, which reduced the electron holes and their recombination which prolongs the life-

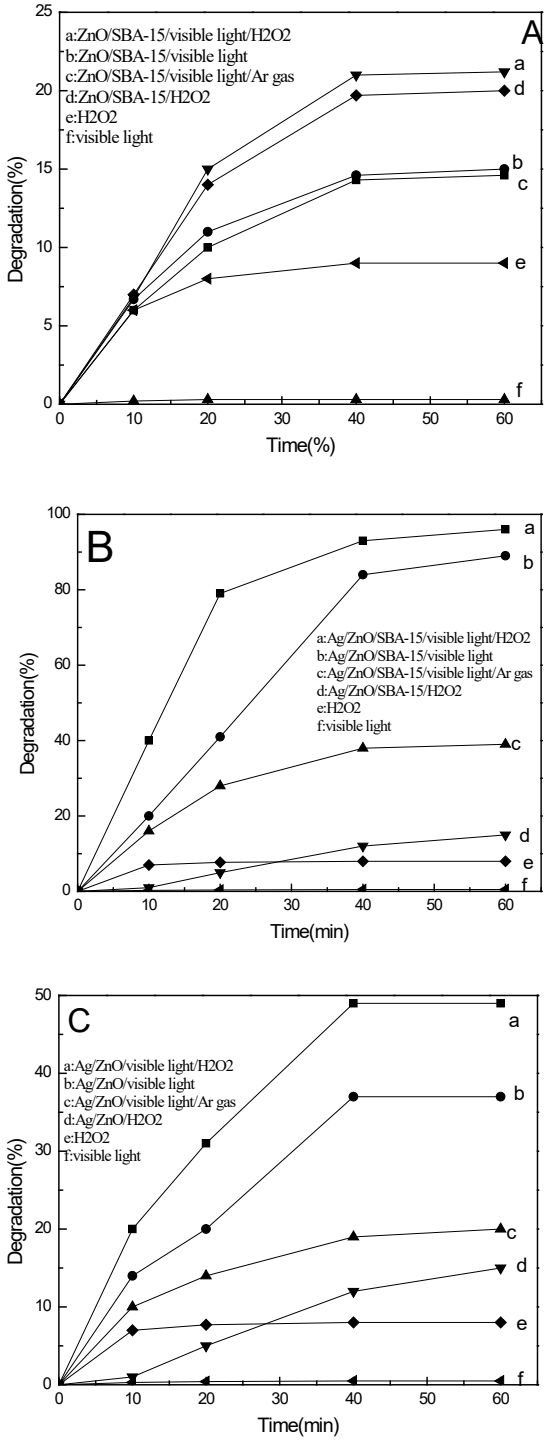

Fig. 5. MO degradation. A: ZnO/SBA-15 system; B: Ag/ZnO/SBA-15 system; C: Ag/ZnO system.

times of the generated pairs. Because of surface plasmon resonance (SPR), most of the electrons generated during photo-catalysis were excited from Ag particle surfaces of the conduction band of ZnO, promoting the formation of radicals which enhanced photo-catalytic efficiency. The superoxide radical ($^{\bullet}O_2^-$) was produced because adsorbed

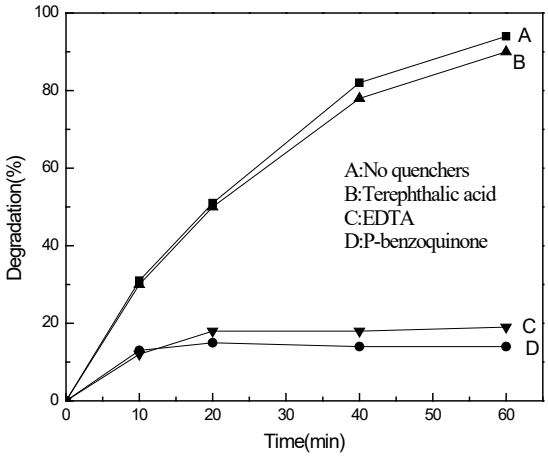

Fig. 6. Photo-catalytic activities of Ag/ZnO/SBA-15 for the degradation of MO with different scavengers.

Table 2
Textual and structural properties of samples

Materials	SBET (m^2/g)	Pore volume (cm^3/g)	Pore size (nm)
SBA-15	590.2	1.22	5.97
ZnO/SBA-15	300.7	0.81	5.69
Ag/ZnO/SBA-15	290.4	0.78	5.48

O_2 readily traps electrons generated during photo-catalysis [25–28] and degrades the MO dye to CO_2 and other intermediate products.

Stability is an important property for photo-catalysts, so in an effort to examine the stability of Ag/ZnO/SBA-15, recycling of the photo-catalyst was tested for MO photo-catalytic degradation (Fig. 7A). Those tests showed only a small drop in activity after five cycles using visible light and demonstrated the stability of these photo-catalysts during liquid-solid heterogeneous irradiation. As shown in Fig. 7B, there was no obvious change in the structure of the Ag/ZnO/SBA-15, suggesting that the sample was stable during photo-catalysis.

4. Conclusions

In this work, a facile two-step method was used to successfully synthesize a Ag/ZnO/SBA-15 composite. The composite material was unambiguously characterized by several spectroscopic techniques. Surface plasmon resonance (SPR) showed enhanced catalytic activity of Ag/ZnO/SBA-15 compared to ZnO/SBA-15 for MO degradation under simulated solar light. Moreover, photo-catalyst recycling experiments proved that Ag/ZnO/SBA-15 composites could be used in practical application of pollutant treatment because of its good stability. These results also suggested that the coupling effect between Ag and ZnO would be valuable in the mineralization for the organic pollutants under solar light.

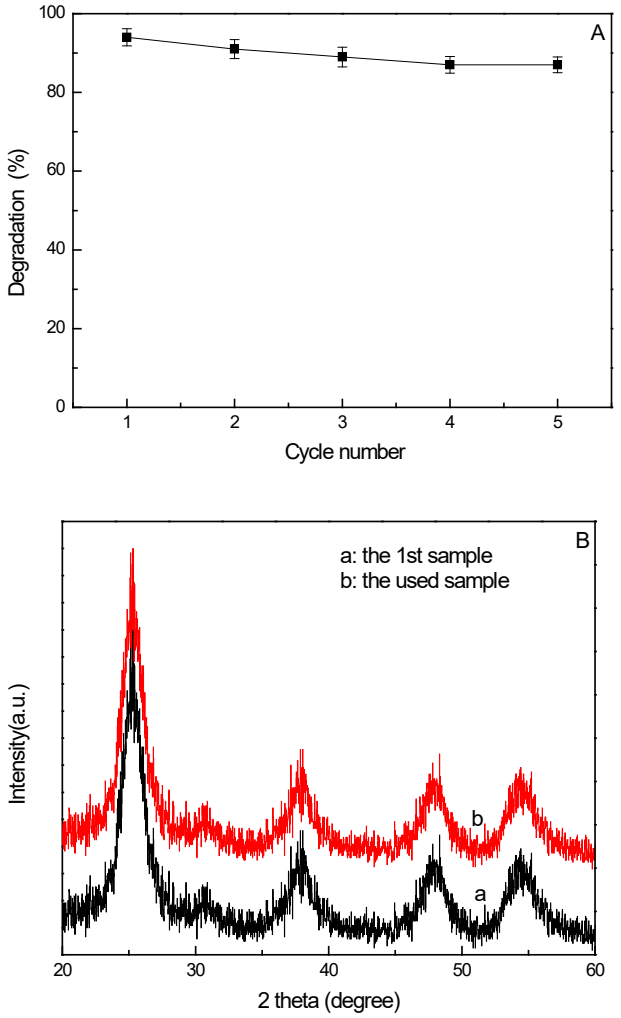

Fig. 7. Sample stability. A: MO degradation by Ag/ZnO/SBA-15 after 5-cycles; B: XRD patterns of Ag/ZnO/SBA-15 before and after the cycles.

Acknowledgements

This research was financially supported by the National Natural Science Foundation of China (Grant No. 51673106), the Program of Science & Research of Shandong Province (2016GSF116005) and the Taishan Scholar Program of Shandong.

References

[1] R. Asahi, T. Morikawa, T. Ohwaki, K. Aoki, Y. Taga, Visible-light photocatalysis in nitrogen-doped titanium oxides, Science, 293 (2001) 269–271.
[2] Y. Zhou, F.S. Liu, S.T. Yu, Preparation and photo-catalytic activities of FeOOH/ZnO/MMT composite, Appl. Surf. Sci., 355 (2015) 861–867.
[3] Y.S. Malghe, A.B. Lavand, Synthesis, characterization and investigation of visible light photocatalytic activity of C, N co-doped ZnO, Mater. Lett., 7 (2016) 181–186.
[4] Y. Zhang, C. Pan, TiO_2/graphene composite from thermal reaction of graphene oxide and its photocatalytic activity in visible light, J. Mater. Sci., 46 (2011) 2622–2626.
[5] J. Wang, S. Yang, X. Liu, Preparation and characterization of ZrO_2 thin film on sulfonated self-assembled monolayer of 3-mercaptopropyl trimethoxysilane, Appl. Surf. Sci., 221 (2004) 272–280.
[6] C. Martinez, M.L. Canle, M.I. Fernández, J.A. Santaballa, J. Faria, Kinetics and mechanism of aqueous degradation of carbamazepine by heterogeneous photocatalysis using nanocrystalline TiO_2, ZnO and multi-walled carbon nanotubes-anatase composites, Appl. Catal. B, 102 (2011) 563–571.
[7] Y.D. Wang, S. Zhang, C.L. Ma, H.D. Li, Synthesis and room temperature photoluminescence of ZnO/CTAB ordered layered nano-composite with flake-like architecture, J. Lumin., 126 (2007) 661–664.
[8] D.Y. Fu, G.Y. Han, Y. Chang, J.H. Dong, The synthesis and properties of ZnO-graphene nano hybrid for photodegradation of organic pollutant in water, Mater. Chem. Phys., 132 (2012) 673–681.
[9] X. Sun, H.X. Yu, D. Zheng, X.S. Wang, J.S. Li, L.J. Wang, Incorporation of nanoscale zero-valent iron particles inside the channels of SBA-15 silica rods by a "two solvents" reduction technique, Appl. Surf. Sci., 279 (2013) 1–6.
[10] J.V.D. Meer, I. Bardezgiboire, C. Mercier, B. Revel, A. Davidson, R. Denoyel, Mechanism of metal oxide nanoparticle loading in SBA-15 by the double solvent technique, J. Phys. Chem. C, 114 (2010) 3507–3515.
[11] W. Choi, A. Terrain, M.R. Hoffman, The role of metal ion dopants in quantum-sized TiO_2 correction between photo reactivity and charge C, J. Phys. Chem., 98 (1994) 13669–13679.
[12] S.C. Yan, Z.S. Li, Z.G. Zou, Photodegradation of rhodamine B and methyl orange over boron-doped g-C_3N_4 under visible light irradiation, Langmuir, 26 (2010) 3894–3901.
[13] D. Zhao, J. Feng, Q. Huo, N. Melosh, G.H. Fredrickson, B.F. Chmelka, G.D. Stucky, Triblock copolymer syntheses of mesoporous silica with periodic 50 to 300 angstrom pores, Science, 279 (1998) 548–552.
[14] M. Anbia, S. Amirmahmoodi, Adsorption of phenolic compounds from aqueous solutions using functionalized SBA-15 as a nano-sorbent, Scientia Iranica., 18 (2011) 446–452.
[15] Y. Zhou, F.S. Liu, Z.Y. Sun, Y.Y. Chu, Preparation and photo-catalytic activities of Ag/FeOOH /SBA-15 composite, J. Photoch. Photobio. A, 336 (2017) 17–24.
[16] A.R. Malagutti, H.L. Mourao, J.R. Garbin, Deposition of TiO_2 and Ag: TiO_2 thin films by the polymeric precursor method and their application in the photo degradation of textile dyes, Appl. Catal. B, 90 (2009) 205–212.
[17] P. Wang, D. Chen, F.Q. Tang, Preparation of titania-coated polystyrene particles in mixed solvents by ammonia catalysis, Langmuir, 22 (2006) 4832–4835.
[18] T.J. Xin, M.L. Ma, H.P. Zhang, J.W. Gu, S.J. Wang, M.J. Liu, Q.Y. Zhang, A facile approach for the synthesis of magnetic separable Fe_3O_4@TiO_2 core-shell nano composites as highly recyclable photo catalysts, Appl. Surf. Sci., 288 (2014) 51–59.
[19] M.K. Lee, T.G. Kim, W. Kim, T. Kin, Y.M. Sung, Surface plasmon resonance (SPR) electron and energy transfer in noble metal-zinc oxide composite nanocrystals, J. Phys. Chem. C, 112 (2008) 10079–10082.
[20] R.F. Dong, B.Z. Tian, J.L. Zhang, T.T. Wang, Q.S. Tao, S.Y. Bao, F. Yang, C.Y. Zeng, AgBr/Ag/TiO_2 core-shell composite with excellent visible light photo-catalytic activity and hydrothermal stability, Catal. Commun., 38 (2013) 16–20.
[21] D.S. Wang, L. Shi, Q.Z. Luo, X.Y. Lei, J. An, An efficient visible light photo-catalyst prepared from TiO_2 and polyvinyl chloride, J. Mater. Sci., 47 (2012) 2136–2145.
[22] C. Hu, T.W. Peng, X.X. Hu, Y.L. Nie, X.F. Zhou, J.H. Qu, H. He, Plasmon-induced photo degradation of toxic pollutants withAg/AgI/Al_2O_3 under visible-light irradiation, J. Am. Chem. Soc., 132 (2010) 857–862.
[23] H. Maki, Y. Okumura, H. Ikuta, M. Mizuhata, Ionic equilibria for synthesis of TiO_2 thin films by the liquid-phase deposition, J. Phys. Chem. C, 118 (2014) 11964–11974.
[24] R.S. Yuan, J.T. Zheng, R.B. Guan, Y.C. Zhao, Surface characteristics and photocatalytic activity of TiO_2 loaded on activated carbon fibers, Colloid. Surf. A, 254 (2005) 131–136.

[25] H. Lachheb, O. Ahmed, A. Houas, Photocatalytic activity of TiO_2-SBA-15 under UV and visible light, J. Photoch. Photobio. A, 226 (2011) 1–8.
[26] L. Shi, L. Liang, J. Ma, Highly efficient visible light-driven Ag/AgBr/ZnO composite photocatalyst for degrading rhodamine B, Ceram. Int., 40 (2014) 3495–3502.
[27] Y.S. Liu, S.H. Wei, W. Gao, Ag/ZnO heterostructures and their photocatalytic activity under visible light: effect of reducing medium, J. Hazard. Mater., 287 (2015) 59–68.
[28] Z. Chen, L. Fang, W. Dong, Inverse opal structured Ag/TiO_2 plasmonic photocatalyst prepared by pulsed current deposition and its enhanced visible light photocatalytic activity, J. Mater. Chem. A, 2 (2014) 824–832.